Title
INVARIANT LINE STRAIN AND NEEDLE-PRECIPITATE GROWTH DIRECTIONS

Authors
Dahmen, U.
Ferguson, P.
Westmacott, K.H.

Publication Date
1983-08-01

Lawrence Berkeley Laboratory

UNIVERSITY OF CALIFORNIA

Materials & Molecular Research Division

Submitted to Acta Metallurgica

INVARIANT LINE STRAIN AND NEEDLE-PRECIPITATE GROWTH DIRECTIONS

U. Dahmen, P. Ferguson, and K.H. Westmacott

August 1983

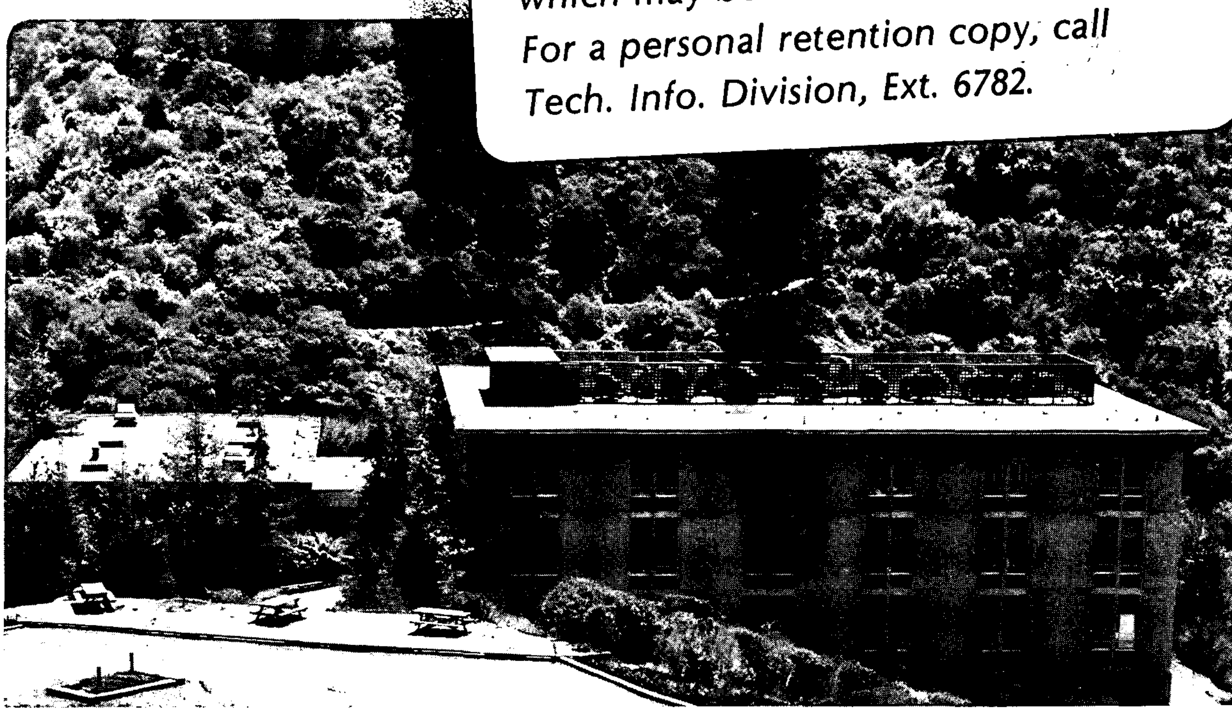

Prepared for the U.S. Department of Energy under Contract DE-AC03-76SF00098

Invariant Line Strain and Needle-Precipitate Growth Directions

U. Dahmen, P. Ferguson and K. H. Westmacott
Materials and Molecular Research Division
Lawrence Berkeley Laboratory
University of California
Berkeley, California 94720

ABSTRACT

A detailed theory of precipitate needle growth based on the invariant line hypothesis is presented for fcc $\rightleftharpoons$ bcc alloy systems. The basic concept that coherent needle axes lie on cones of unextended lines is applied to semicoherent needles and it is shown that loss of coherency and growth is possible only for those needles lying at the intersection of a cone of unextended lines with a matrix slip plane. For these needles shear dislocation loops can relieve the coherency stresses. Owing to the different slip geometries, <561> needle directions clustered around <110> directions are predicted for bcc Cr precipitate needles in an fcc Cu matrix, and <557> and <656> directions clustered around <111> for the inverse case of fcc Cu in bcc Fe. Precise experimental measurements on both the alloy systems are in excellent agreement with the predictions. Differences observed in the incidence of <557> and <656> needles in Fe-Cu are related to the relative efficiency of the available matrix slip systems in providing transformation strain relief. It is concluded that the two factors that govern the precipitate crystallography are strain minimization and crystallographic strain relief.

1. Introduction

One of the simplest precipitate morphologies, needle- or rod-like, arises from low misfit along the needle axis. Recently Weatherly et al. (1) found that in Cu-Cr alloys precipitate needles of bcc Cr were oriented along high-index directions of the fcc Cu matrix. In another recent study of surface precipitation in Cu-Zn, Crosky et al. (2,3) reported large fcc needles on the surface of the bcc matrix lying along directions of no strain. A detailed crystallographic analysis of the orientation relationships and directions of individual needles revealed that these precipitates were related to the matrix by an invariant line strain. The same conclusion was reached in a study of orientation relationships for a large number of different alloy systems (4).

A model based on the invariant line hypothesis was subsequently outlined (5), and the predictions matched the published results on Cu-Cr and Cu-Zn alloys. From a knowledge of the crystal structures involved and their ratio of lattice parameters alone, three simple predictions for needleshaped precipitates were made:

1) coherent needles lie on the cone of unextended lines as given by the stress-free transformation strain.

2) semicoherent needles lie along the intersection of the cone of unextended lines with a matrix slip plane.

3) surface needles lie along the intersections of the cone of unextended lines with the surface.

The first two points apply to bulk precipitation and were shown to agree with the experimental results on Cu-Cr. The third point was made explicitly by Crosky et al. in the study on Cu-Zn and applies to surface precipitation.

In the present paper a full theory of needle growth based on the invariant line hypothesis is developed for bulk precipitation. To test its generality, the predictions of the theory are compared with observations on Fe-Cu, a system that is inverse to Cu-Cr in that the role of matrix and precipitate crystal structure is interchanged.

2. Model

The principles underlying the proposed model are that the precipitate will adopt a morphology that (1) minimizes the growth strains and (2) maximizes the conditions for crystallographic relief of those strains. The first criterion can be formulated in terms of continuum concepts, while the second makes the connection with the discrete lattice.

It is well-known that whenever the three principal strains describing the structural part of a phase transformation include two strains of opposite sign, there will be a set of vectors which remain unextended during the transformation. These vectors $\underline{u}$ are given by the condition $|\hat{B}\underline{u}| = |\underline{u}|$ i.e. the magnitude of $\underline{u}$ is unchanged by the transformation $\hat{B}$. Fig. 1 illustrates this for the 2-dimensional case. The unit circle $\underline{u}$ is transformed into the ellipse of axes a and b by the transformation $\hat{B} = \begin{pmatrix} a & 0 \\ 0 & b \end{pmatrix}$. The principal strains a-1 and b-1 have opposite sign, and hence the unextended vectors $\underline{u}$ which transform into $\underline{v} = \hat{B}\,\underline{u}$ are given by

$$a^2 u_x^2 + b^2 u_y^2 = u_x^2 + u_y^2 \; .$$

The angle α of the unextended lines with the x-axis is given by

$$\tan \alpha = \frac{u_y}{u_x} = \frac{a^2-1}{1-b^2} .$$

In the 3-dimensional case, a unit sphere transforms into an ellipsoid of axes a,b,c under the transformation $\hat{B} = \begin{pmatrix} a & 0 & 0 \\ 0 & b & 0 \\ 0 & 0 & c \end{pmatrix}$ and the unextended lines form a cone.

For the Bain strain appropriate to the present case $\hat{B} = \begin{pmatrix} a & 0 & 0 \\ 0 & c & 0 \\ 0 & 0 & a \end{pmatrix}$, the cone has circular cross section and is centered on the [010] axis as shown in the stereograms in Fig. 2a and b for Fe-Cu and Cu-Cr respectively.

Any unextended vector will undergo a rotation during the transformation bringing it from the initial to the final cone of unextended lines. If one of the unextended vectors is rotated back to its initial position by a rigid body rotation $\hat{R}$, then this one vector is an invariant line of the transformation and the transformation strain $\hat{A} = \hat{R}\hat{B}$ is an invariant line strain. The invariant line $\underline{u}$ is neither stretched nor rotated by the transformation $\hat{A}$ so that

$$\hat{A}\underline{u} = \underline{u} .$$

There is no misfit between the two lattices along this line so that a needle-shaped precipitate would naturally grow along this direction.

A second effect of the rotation $\hat{R}$ is illustrated in Figs. 1c, d where the strains are shown as arrows. From the figure it is apparent that the same rotation that makes an unextended line into an invariant line changes the compressive and dilatational strains of Fig. 1c into the shear strain of Fig. 1d with all strain vectors taking the same direction. An invariant line rotation is thus seen to convert part of the transformation strains into simple shear.

Any unextended line can be made an invariant line by the appropriate rotation. In the absence of other constraints, precipitate needles could therefore lie anywhere on the cone of unextended lines. This was indeed found to be the case for coherent Cr needles in Cu which are distributed on cones centered on the three <100> directions (1).

Coherent growth can occur until the stresses that develop normal to the invariant line reach a critical value. At this point the crystallographic restriction is imposed and only those precipitates favorably oriented for nucleating a shear loop will lose coherency and continue to grow. The Burgers vector of the shear loop will be opposite in sign to the coherency strains so as to counter the strain and permit further growth. Whether the loop is nucleated and propagated in the precipitate or matrix should depend on the respective shear moduli. Since only a small fraction of the coherent needles grow while the remainder shrink, this stage is marked by a change in the precipitate size, orientation and distribution, and is thus readily detected experimentally.

The alloy systems Fe-Cu, together with Cu-Cr studied previously (1) were chosen to test the model. Fe-Cu is a simple binary system known to form needle-shaped precipitates (6,7). As for Cr in Cu the solubility of Cu in Fe is low, and during precipitation above 600°C the alloy separates into the pure constituents. The ratio of the lattice parameters is almost identical for Fe-Cu and Cu-Cr. Thus, with regard to the model, the only significant difference between the two alloys is that in the present case (Fe-Cu) fcc needles form in a bcc matrix instead of bcc needles in an fcc matrix (Cu-Cr) leading to different slip plane symmetry. As a consequence the predicted invariant line directions given by the intersections of the cone of unextended lines with the slip planes will be <557> or <656> in Fe-Cu, rather than the <651> in Cu-Cr. Figs. 2a, b illustrate these intersections for Fe-Cu and Cu-Cr, respectively. For clarity, only one variant of the Bain distortion with its single cone of unextended lines centered on [010] is drawn. The intersections with the vertical ($\bar{1}01$) and (101) planes in Fig. 2a have indices <656> and are shown as solid circles and the intersections with the inclined {110} planes have indices <557> and are shown as open circles. If the other two variants of the cone of unextended lines (centered on [001] and [100]) are taken into account, a complete set of invariant line directions is obtained as shown in Figs. 2c, d. For Fe-Cu the invariant lines cluster in two groups of three (open and solid circles) around the <111> directions (Fig. 2c) whereas for Cu-Cr they form clusters of four around the <110> directions (Fig. 2d). A comparison of the directions predicted for Cu-Cr illustrated in Fig. 2d with those experimentally observed by Weatherly et al. (Fig. 2b in Ref. (1)) shows good agreement. The corresponding predictions for Fe-Cu are shown in (Fig. 2c) and are tested by the present results.

3. Experimental Procedure

3.1. Specimen Preparation. A hot-rolled Fe-2wt%Cu strip 0.15mm thick was abraded, electropolished and annealed 24h at 1000°C in hydrogen. The as-annealed material was solution-treated 16h at 850°C in a vacuum furnace evacuated to < 2.7mPa and quenched into silicone oil at room temperature. Specimens were subsequently aged in the vacuum furnace. Thin foils of the aged material were prepared by the window technique in a 68vol% acetic acid: 16vol% 2-butoxyethanol: 16vol% perchloric acid electrolyte at 25-30°C using 20 volts and a current density of 0.1 amp cm^{-2}. Electron microscopy was performed using a Siemens 102 and Kratos 1.5MeV microscope operating at 100 and 300kV respectively.

3.2. Crystallographic analysis of precipitate needles. The standard method of determining the axes of precipitate needles is by trace analysis. In the present case, it was more convenient to test directly the predictions of the theory by comparing the projected needle directions plotted on a stereogram with micrographs taken in the same orientation. This method which takes advantage of the symmetry of the matrix crystal, allows the needle directions to be rapidly classified and a statistically significant analysis to be made.

Considering for the present only the <557> needle variants (open circles in Fig. 3a), it can readily be seen that for the bcc/fcc case, a foil oriented with a <110> direction parallel to the electron beam is optimum since it brings six of the twelve needle variant axes in or near the plane of the projection. Of the twelve variants, only seven distinguishable projections appear due to the crystal symmetry. Six of these are related by mirror symmetry across $(\bar{1}10)$ as shown in Fig. 3b.

The enclosed angles between the projected directions X-X', Y-Y' and Z-Z' are 118.5°, 91.5° and 29.2° respectively. If precipitate needles with the preceding <557> angular relationships or the alternative <656> directions are found, and no other, the model can be considered confirmed.

4. Results

Fig. 4a shows a typical field of precipitate needles found after aging for 16h at 750°C. A network of dislocations that was not introduced during specimen preparation connects the precipitates which at first sight appear almost randomly distributed. However, when the dislocations are out of contrast, as in Fig. 4b, and only some precipitate variants are strongly diffracting, an alignment of the needles along certain directions becomes apparent.

Fig. 5 was taken in an exact [110] beam direction thus allowing a direct comparison with the needle trace pattern from Fig. 3b. The trace of the $(\bar{1}10)$ mirror plane is indicated by a solid line. Several precipitates marked M are seen to lie exactly parallel to this line. They may be recognized by their Moiré fringes, a high aspect ratio, and rounded ends. These variants are clearly distinguishable from the ones marked X and their "mirror images" X', which have strong contrast, are wide and have squared-off ends. The measured angle between the X and X' variants agrees exactly with that predicted (118.5°). This is the most accurate measurement since X and X' lie in the plane of the micrograph. Y and Y' precipitates are similar in shape and contrast to X and X' and enclose the predicted angle of 91.5°. Comparison with Fig. 3 shows that they lie close to the plane of the projection.

A less accurate measurement is obtained for the steeply inclined precipitates Z and Z' since they appear short in this projection. But again the measured angles agree with those predicted (29.2°). Finally, as expected, the M precipitates are seen to bisect the angles between all the other variants, X and X', Y and Y', Z and Z'.

Further morphological information is obtained from the projected shapes of these <557> needles. Their true shape may be derived from the two needle projections M and X (or X'). The ratio of length ℓ to thickness t is seen in the M precipitates with the length foreshortened by the ~45° inclination. The ratio of ℓ to width w is obtained directly from the X (or X') precipitates. Mean values averaged over more than 150 particles are $\ell/t = 4.4$ and $\ell/w \doteq 2.4$.

568 of the total number of 586 precipitates measured coincided with the predicted directions, confirming that the majority of the needles are of one and the same crystallographic type. However, 18 clearly did not conform to the pattern. One such particle is arrowed in Fig. 6 where the same symbols as in Figs. 3 and 5 denote the different variants. An analysis of these needles showed them to lie in <656> directions, the intersection of the vertical {110} planes with the cone of unextended lines. From Figs. 2 and 3 it is seen that the two needle types, <557> and <656> lie at angles of ~9° and ~5° respectively, from the <111> directions on the {110} planes.

In Fig. 3a several variants of the second type (solid circles) are seen to project into directions which are close, or identical to those of the first type (open circles). For example, the $(\bar{1}10)$ mirror plane contains directions of both types (solid and open circles).

The directions which are most easily and accurately recognized as the second type of needle are clearly the ones located between the X and the Y particles, one of which is arrowed in the stereogram of Fig. 3a and in the micrograph of Fig. 6. Because of the partial overlap of the projected directions of the two types of needle, their relative frequency of occurrence must take into account only those needles which are unambiguously of one kind or the other. With this precaution, it was found that only about 5% of the needles were of the <656> type and all others were of the <557> type.

5. Discussion

The successful interpretation of the present experimental results in terms of the proposed model together with the earlier excellent agreement found for the Cu-Cr data suggests a general validity of the model for this class of alloy system. Interchanging the bcc and fcc crystal structures between matrix and precipitate alters the symmetry of the slip systems but the same principles are found to hold.

It is interesting that of the two possible types of needle direction predicted for the bcc ⟶ fcc case, one, the <557>, was overwhelmingly favored over the other, the <656>. This disparity in occurrence can be related to the optimization of the coherency stress relief. If this loss of coherency is possible only by a conservative process, it must occur by slip, as for example in the nucleation of a shear dislocation loop or by interaction with an appropriate existing lattice dislocation. For such dislocation shear to counteract the transformation strains efficiently, it is necessary:

1) to convert as large a part as possible of the transformation strain into simple shears

and

2) for these shear strains to lie on crystallographic shear systems, i.e. low-index planes.

The first requirement is particularly important in the present case since the transformation from a bcc structure with the lattice parameter of Fe to an fcc structure with the lattice parameter of Cu involves almost no change in atomic volume. Hence the large strains of the Bain correspondence can be converted almost entirely into simple shears by appropriate rotations between matrix and precipitate lattices. This is shown for the case of the <656> needles in Fig. 7a. The {110} slip plane of the bcc matrix lattice is outlined as a solid rectangular lattice and the {100} plane of the precipitate is shown as a dashed square lattice. To produce the indicated invariant line, the two lattices are rotated relative to each other by 9.3°. The resulting strain in this slip plane takes on a predominantly shear character and increases with distance from the invariant line as emphasized by the arrows representing the strain below the invariant line in Fig. 7a.

The orientation relationship corresponding to this is $(101)_{bcc} \| (001)_{fcc}$ and $[010]_{bcc}$ 9.3° from $[010]_{fcc}$ which is within 0.5° of the Pitsch relationship. These needles meet both of the demands given above; they convert the transformation strains into simple shear and ensure that this shear lies in the $\{110\}_{bcc}$ slip plane. However, the conversion of positive and negative strains into simple shear is incomplete. This is evident in Fig. 7a where the arrows giving the direction of the shear strain in the $\{101\}_{bcc}$ plane are not parallel to the invariant line, signifying a residual expansion component (12.5%). At the same time the strain normal to the plane of the projection is an 11% contraction. If a further rotation between the two lattices could convert these two opposite strains into a second simple shear, the strain conversion would be more complete. This requires a different orientation relationship and a different invariant line and the result is shown in Fig. 7b.

The same {110} matrix projection as in Fig. 7a is shown by the same rectangular solid lattice. However, it is now parallel to the $\{111\}_{fcc}$ plane (dashed rectangular lattice). When rotated to produce an invariant line, the <557> direction of the majority needles is obtained. The rotation between the lattices is 5.75° in agreement with the experimentally observed orientation relationship shown in Fig. 8b obtained by selected area diffraction from the <557> precipitate shown in Fig. 8a. This is within 0.5° of the Kurdjumov-Sachs relationship previously reported by Speich and Oriani (7) and may be described as $\{110\}_{bcc} \| \{111\}_{fcc}$ and $\langle 001\rangle_{bcc}$ 5.26° from $\langle \bar{1}01\rangle_{fcc}$. Note that the rotation between the lattices is in the opposite sense to Fig. 7a and that the strain vectors in the plane of the drawing are almost parallel to the invariant line. Hence in this projection the transformation strain is close to a simple shear, modified only slightly by a small residual contraction (2.5%) with only a small orthogonal expansion (3%). Apart from these small residual strains, the transformation for this orientation relationship is entirely described by two simple shears on low-index planes. Thus the coherency stresses of needles with this orientation can be relieved efficiently by crystallographic shear, leaving only small residual strains to be accommodated elastically. This explains why the <557> needles are favored over the <656> needles whose single shear permits only a less complete plastic accommodation. It is interesting to note that formally the two shears of the majority needles are almost identical to those invoked by Kurdjumov and Sachs in their mechanism for the fcc —> bcc transformation (8). The only difference is in the second shear which in the present case is restrained to produce an invariant line. The similarity of the transformation strains to those of the Kurdjumov-Sachs mechanism was also used by Weatherly <u>et al</u>. in their analysis of coherent precipitates in Cu-Cr. They performed computer image simulations to show that the coherency strains of the Cr needles could be approximated by dislocation dipoles. The effective Burgers vector of the dipole was found by adding equal numbers of the two partial dislocations which describe the two shears of the Kurdjumov-Sachs mechanism. They were careful, however, not to attach any physical significance to this mechanism using it only as a formal way of representing the transformation. It is now clear that in the present case of semicoherent needles these homogeneous shears are accommodated by dislocation shear and thus have real significance. Christian has reviewed single and double shear mechanisms for structural transformations (9) and concluded that their role is restricted to the nucleation stage of a martensitic transformation. The importance of the single shear for the <656> needles and the double shear for the <557> needles described above is not in the nucleation of the (diffusional) transformation to the new structure but in the accommodation of the transformed inclusion by plastic deformation.

Precipitates oriented for coherency loss by single or double shear can, of course, always be analyzed as though they were formed by a single or double shear transformation in the opposite sense of shear. In other words, the strains created by a double shear transformation are relieved by the opposite double shear deformation.

One further feature of the micrographs is consistent with the proposed model. The high density of dislocations interconnecting the precipitate needles, evident only in the thick sections transparent at higher accelerating voltages, (Fig. 4) are clearly related to the process of coherency loss. Their presence throughout the matrix suggests that the shear loops are nucleated in the matrix-precipitate interface but expand into the matrix (rather than the precipitate). Other particles in the vicinity with coherency strains opposite in sign to those of the dislocation will attract the dislocation and incorporate it in their interface structures. Efficient use is thus made of all the available lattice dislocations.

6. Summary and Conclusions

1. A model for needle precipitate growth is developed based on the invariant line hypothesis. The two factors governing the precipitate orientation are minimum transformation strain and efficient strain accommodation.
2. For fcc $\rightleftharpoons$ bcc alloy systems the needle axes are predicted to lie along the intersections of the cones of unextended lines with the matrix slip planes.
3. In the case of Fe-Cu (fcc needles in bcc matrix), the predicted directions are $\langle 557\rangle$ and $\langle 656\rangle$ clustered in groups of three about $\langle 111\rangle$ and are accurately confirmed by the experiments. In the inverse case of Cu-Cr (bcc needles in fcc matrix) the $\langle 561\rangle$ predicted directions group in fours about the $\langle 110\rangle$ directions and have also been confirmed by experiment.
4. A much greater incidence of $\langle 557\rangle$ needles than $\langle 656\rangle$ needles is explained by the more complete accommodation of homogeneous transformation strain during coherency loss of the $\langle 557\rangle$ needles.

7. Acknowledgements

We thank Dr. R. M. Fisher for donating the Fe-Cu alloy and for stimulating discussions. This work is supported by the Director, Office of Energy Research, Office of Basic Energy Sciences, Materials Sciences Division of the U. S. Department of Energy under Contract No. DE-AC03-76SF00098.

References

1. G. C. Weatherly, P. Humble and D. Borland, Acta Met. 27, 1815 (1979).
2. A. Crosky, P. G. McDougall and J. S. Bowles, Acta Met. 28, 1495 (1980).
3. A. Crosky, P. G. McDougall and J. S. Bowles, Acta Met. 31, 603 (1983).
4. U. Dahmen, Acta Met. 30, 63 (1982).
5. U. Dahmen and K. H. Westmacott, Proc. Conf. Solid-Solid Phase Transf., Pittsburgh (1981), p. 433.
6. E. Hornbogen, Precipitation from Iron Based Alloys, G. R. Speich, and J. B. Clark, eds., Gordon and Breach, N. Y. 1965, p. 1.
7. G. R. Speich and R. A. Oriani, Trans. AIME 233, 623 (1965).
8. G. Kurdjumov and G. Sachs, Z. Phys. 64, 325 (1930).
9. J. W. Christian, J. Less-Comm. Metals 28, 67 (1972).

Figure Legends

Fig. 1. (a) Schematic representation of the transformation $\hat{B}$ transforming a circle into an ellipse. The two vectors show an unextended line before and after the transformation. (b) A small rotation makes the unextended line into an invariant line. (c) The same transformation as in (a) with vectors indicating positive and negative strains. (d) The same lattice rotation as in (b) aligns all the strain vectors in one direction approximating a simple shear.

Fig. 2. Stereograms showing predicted needle directions at slip plane intersections with a cone of unextended lines (a) in Fe-Cu and (b) in Cu-Cr. Only $\langle 651 \rangle$ intersections occur in Cu-Cr (b) while Fe-Cu shows two types of intersection, $\langle 557 \rangle$ (open circles) and $\langle 656 \rangle$ (solid circles). In (c) and (d) the full set of directions is shown for each of the two alloys when all three cones of unextended lines are taken into account. Fe-Cu exhibits two sets of threefold clusters around $\langle 111 \rangle$ directions (c) while Cu-Cr shows a single set of fourfold clusters around $\langle 110 \rangle$ directions.

Fig. 3. (a) Predicted needle directions in Fe-Cu in a [110] stereogram with symbols as in Fig. 2. In (b) the projected directions of the $\langle 557 \rangle$ needles (open circles) are marked X, X', Y, Y', Z, Z' and M. The M variant lies on the $(\bar{1}10)$ mirror plane which bisects the angles between the other variants, e.g. Z and Z'.

Fig. 4. Typical distribution of Cu needles after aging 16h at 750°C. Note interconnecting dislocations and random appearance of needle directions in (a). The same field of view in (b) with the

dislocations out of contrast suggests an alignment of some of the particles.

Fig. 5. Distribution of Cu precipitates in a [110] zone. The needle directions can be compared directly with those predicted in Fig. 3. Note Moiré fringes along precipitates marked M. The aspect ratio is low for Z and Z' and high for M variants. Only <557> needles corresponding to open circles in Figs. 2 and 3 are apparent.

Fig. 6. Similar field as seen in Fig. 5 in [110] orientation showing evidence for <656> precipitate, see arrow. The projection of this needle lies between X' and Y' (compare to solid circles near perimeter of stereogram in Fig. 3a).

Fig. 7. <656> (a) and <557> (b) invariant lines shown by superposition of a {110} plane of Fe with a {100} Cu plane in (a) and a {111}Cu plane in (b). The necessary rotation between the lattices is 9.3° in (a) and 5.75° in (b) creating orientation relationships within 0.5° of the Pitsch (a) and Kurdjumov-Sachs (b) relationships. The arrows below the invariant line indicate the transformation strains. The strain in (b) is almost entirely a simple shear whereas in (a) an expansion component is evident. The $\langle 557\rangle_{bcc}$ direction shown in (b) is more favorable for the loss of coherency and is equivalent to the $\langle 651\rangle_{fcc}$ direction observed in Cu-Cr.

Fig. 8. (a) Cu precipitate along a <557> invariant line (Y in fig. 3b) with the corresponding selected area diffraction pattern correctly oriented. The matrix orientation is $[110]_{bcc}$ and the precipitate orientation is $[111]_{fcc}$, outlined by a white hexagon. The spots inside the hexagon are caused by double diffraction and surface

oxides. The misorientation between the two patterns is about 5.5°, in agreement with the predicted 5.75° and close to the 5.26° of the Kurdjumov-Sachs relationship.

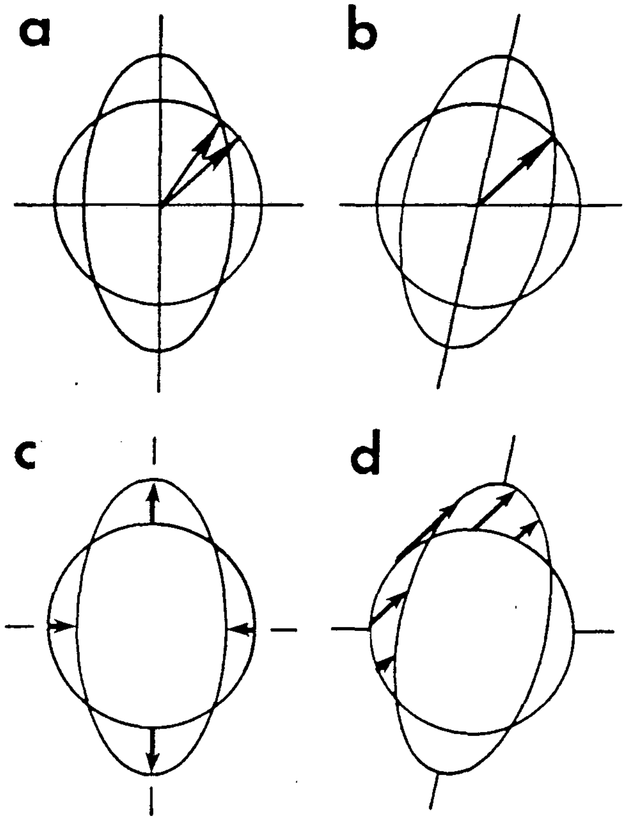

XBL 838-10900

Fig. 1

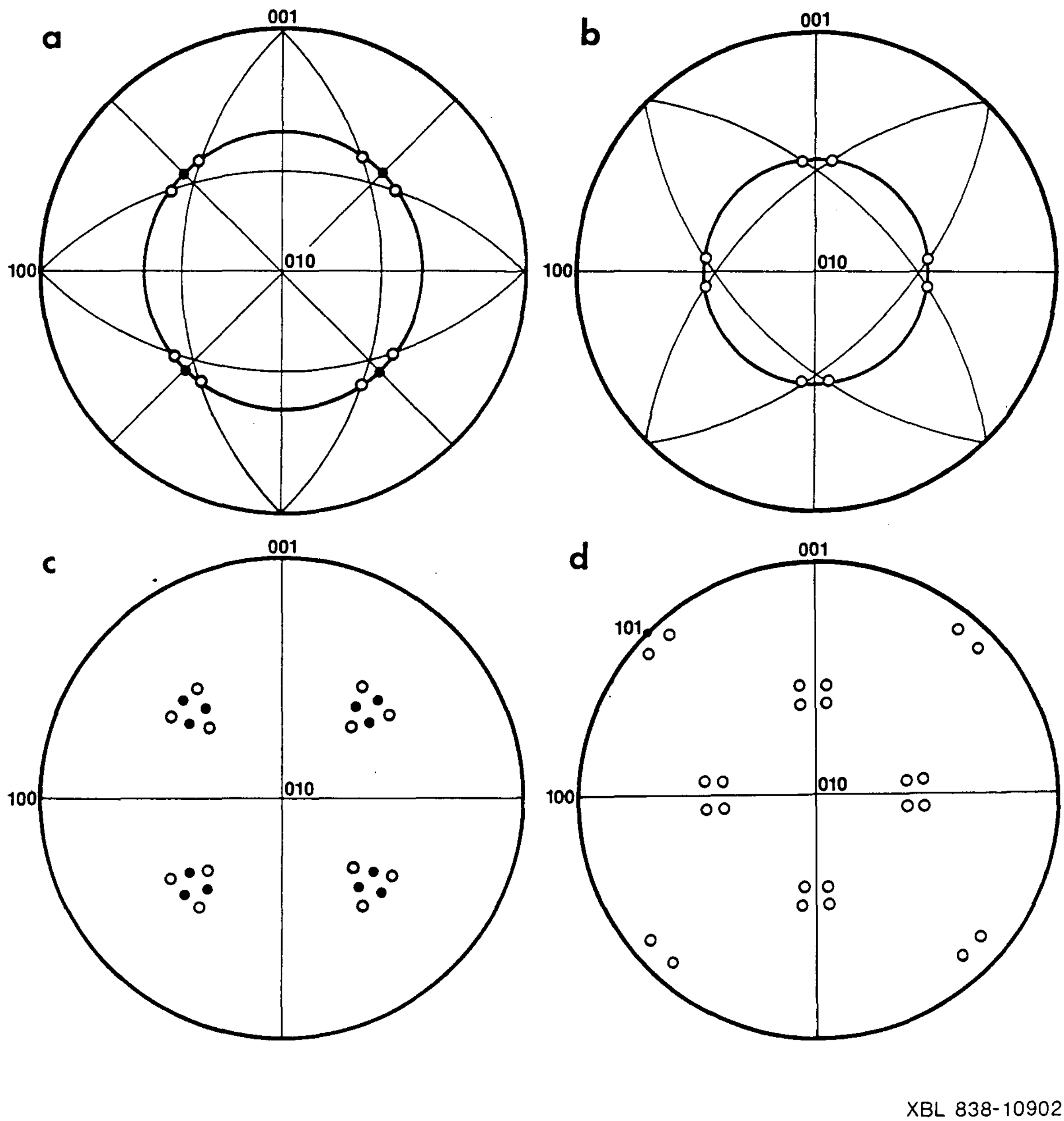
a
001
100
010
b
001
100
010
c
001
100
010
d
001
101
100
010
XBL 838-10902

Fig. 2

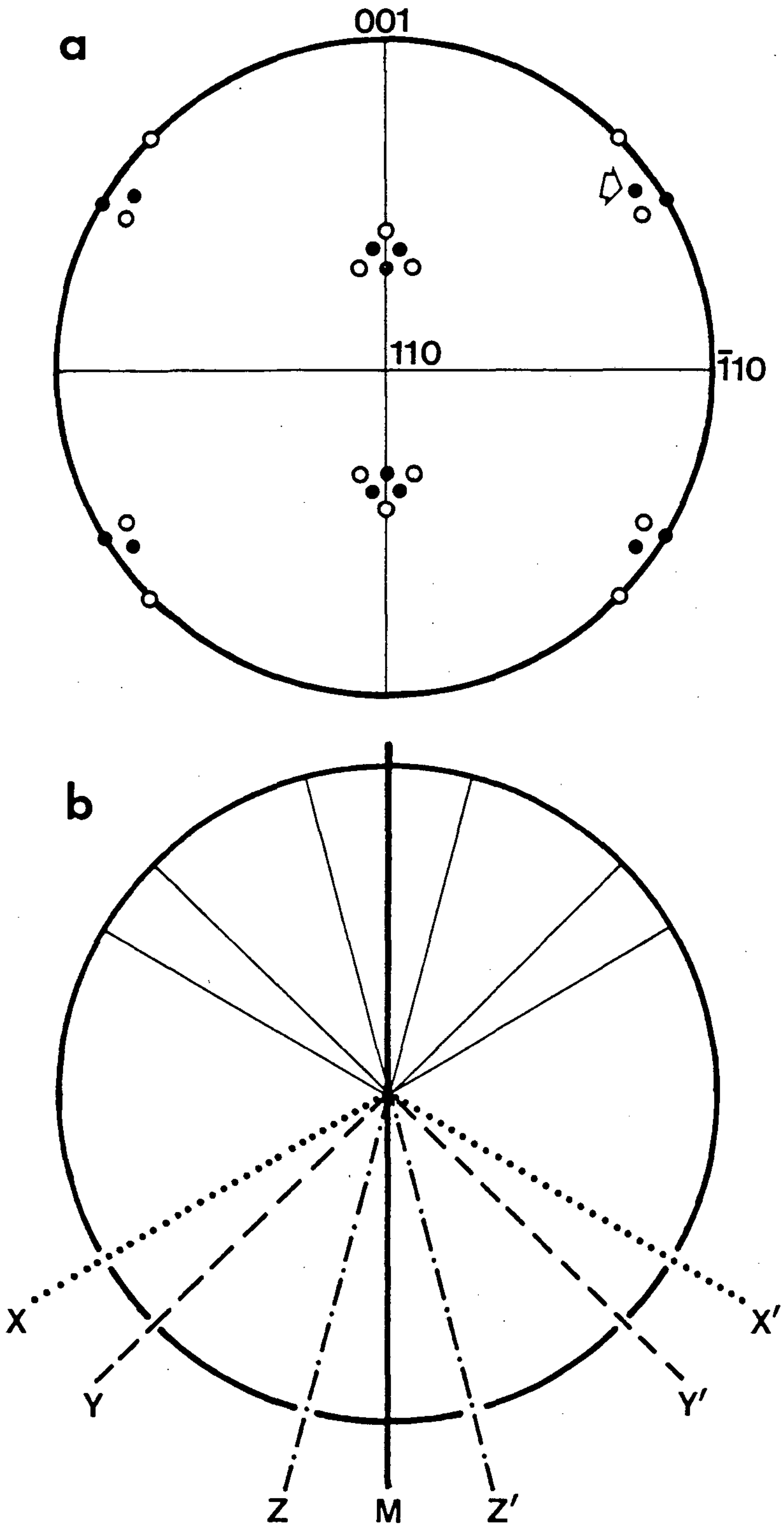

XBL 838-10901

Fig. 3

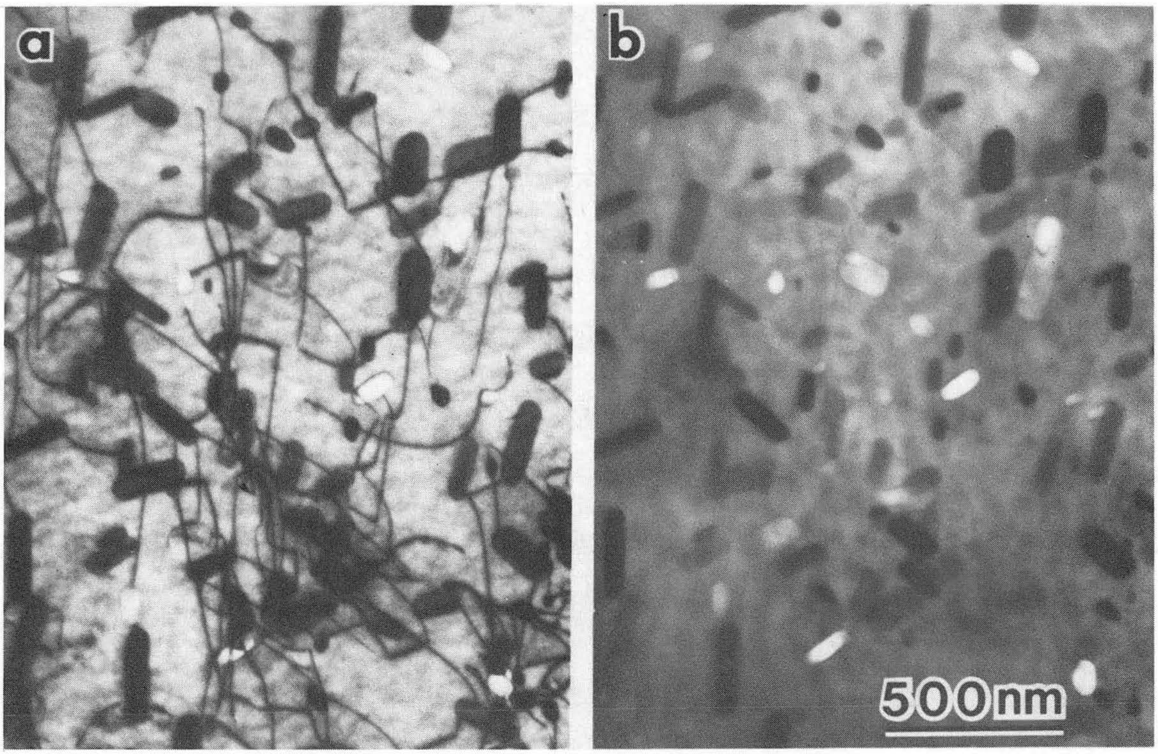

Fig. 4

XBB 837-6655

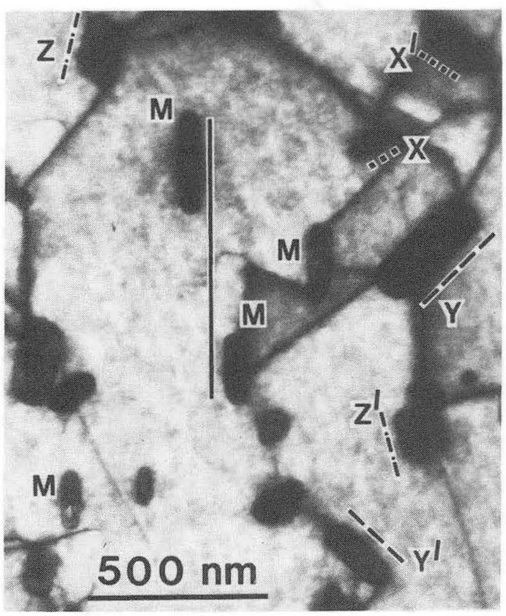

XBB 837-6653

Fig. 5

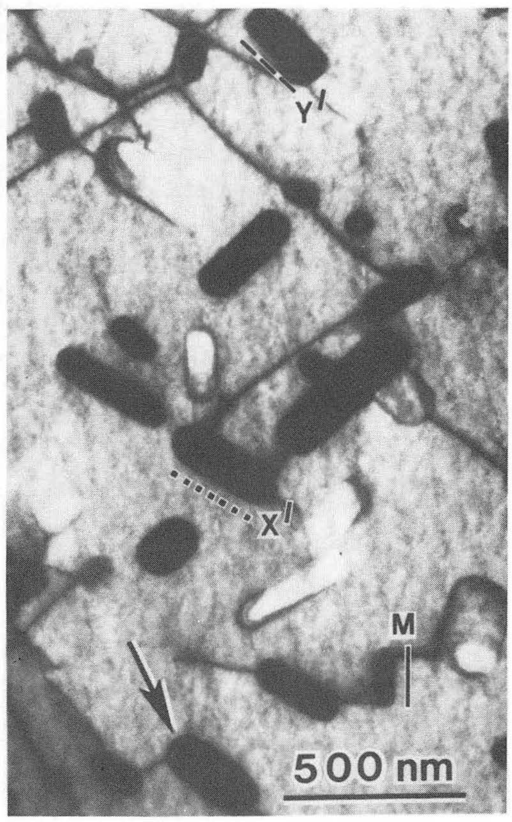

XBB 837-6654

Fig. 6

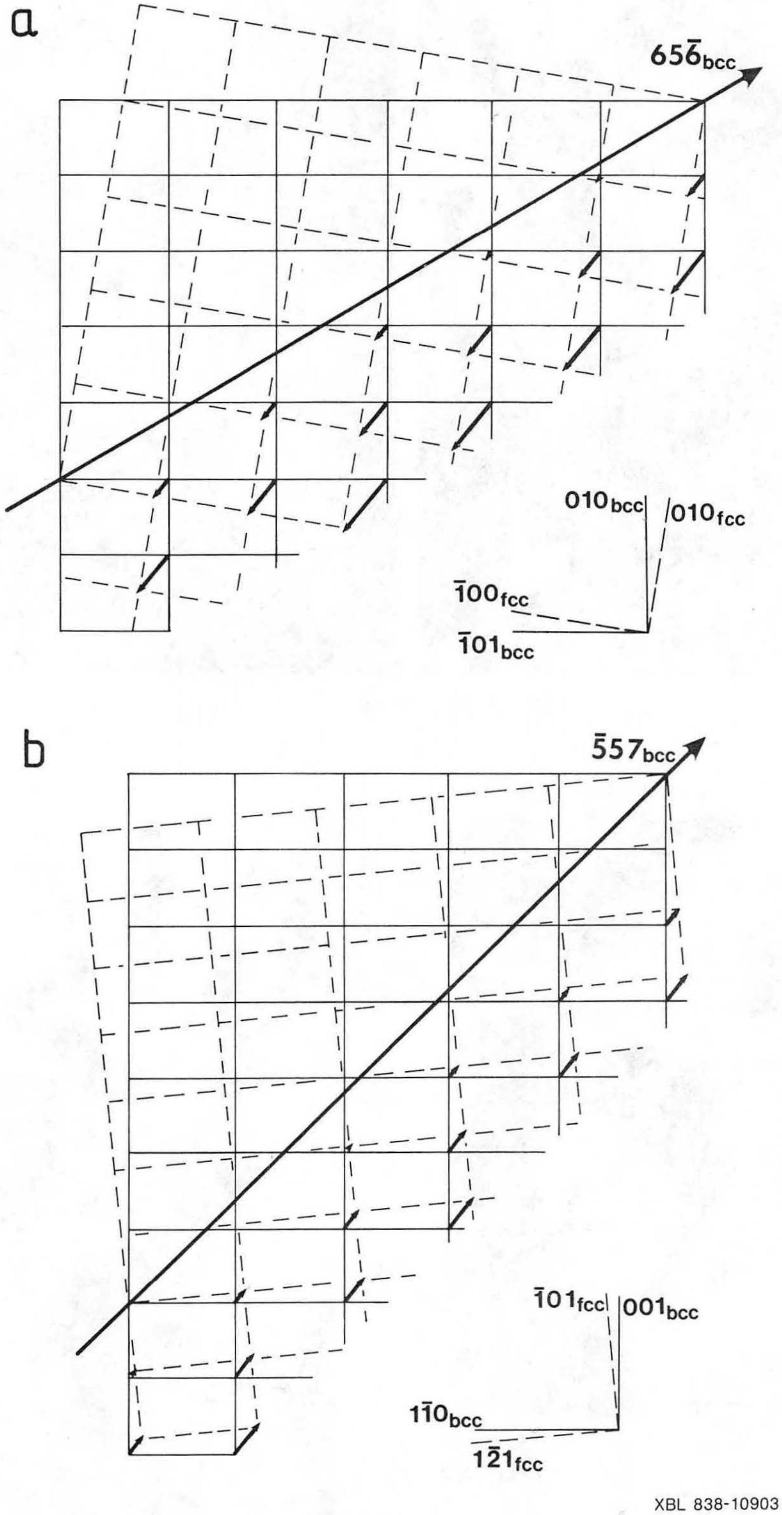

a
$65\bar{6}_{bcc}$
010_{bcc}
010_{fcc}
$\bar{1}00_{fcc}$
$\bar{1}01_{bcc}$
b
$\bar{5}57_{bcc}$
$\bar{1}01_{fcc}$
001_{bcc}
$1\bar{1}0_{bcc}$
$1\bar{2}1_{fcc}$
XBL 838-10903

Fig. 7

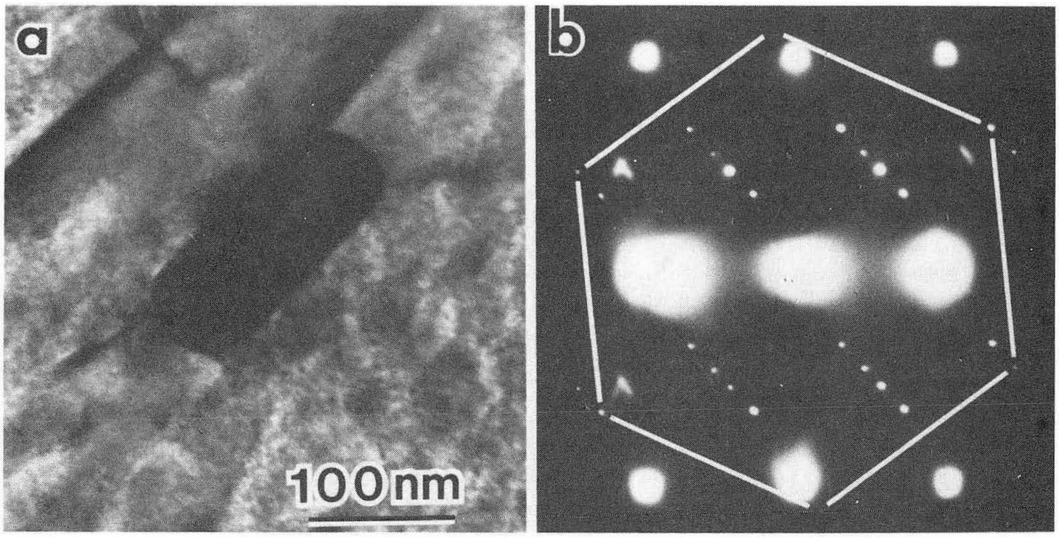

XBB 837-6656

Fig. 8

TECHNICAL INFORMATION DEPARTMENT
LAWRENCE BERKELEY LABORATORY
UNIVERSITY OF CALIFORNIA
BERKELEY, CALIFORNIA 94720